

## Review article

## Roles of surfactants in perovskite solar cells

Abdullah Alasiri<sup>a</sup>, Khalid Zubair<sup>a</sup>, Shazzad Rassel<sup>b</sup>, Dayan Ban<sup>b</sup>, Omar D. Alshehri<sup>c,\*</sup>

<sup>a</sup> Mechanical Engineering Department, King Saud University, Riyadh, Saudi Arabia

<sup>b</sup> Electrical and Computer Engineering Department, Waterloo Institute for Nanotechnology, University of Waterloo, Waterloo, Canada

<sup>c</sup> Industrial Engineering Department, King Saud University, Riyadh, Saudi Arabia



## ARTICLE INFO

## Keywords:

Perovskite solar cells (PSCs)

Surfactants

Coverage area

Crystal orientation

Grain size

Pinholes

## ABSTRACT

In photovoltaics, perovskite solar cells (PSCs) have shown efficiency improvement with scalable and low-cost fabrication. This work investigates the additions of surfactants to PSCs during and after cell fabrication, and how these surfactants enhance the performance of both PSCs and hybrid PSCs. Various types of surfactants were surveyed, including amphoteric, cationic, and non-ionic, in addition to other chemicals that are showing surfactant-like behavior. Surfactants were found to improve coverage area, and reduce roughness, defects, oxygen, moisture and pinholes. They also provided better control over film thickness, grain/spherulite size, and crystal orientation. The mechanisms behind these improvements were explained, and different studies in literature were categorized based on common themes.

## 1. Introduction

Photovoltaic devices (PVs) convert sunlight into electricity, offering a clean and abundant source. The primary goal in PV development is to create low-cost and efficient devices [1,2], which had led to the exploration of various materials, most notably perovskites. In a relatively short period (approximately 9 years), the efficiency of single perovskite solar cells (PSCs) reached 26.1 % [3] – a milestone that took other materials nearly four decades to reach, such as single crystal silicon (26.1 %) [4], multicrystalline silicon (23.3 %) [4], CIGS (Copper Indium Gallium Selenide) (23.35 %) [5], and CdTe (Cadmium Telluride) (22.1 %) [4]. This dramatic increase in efficiency in a short period has made PSCs a focal point for research interest [4].

The term “perovskite” was named after the Russian mineralogist L.A. Perovski and refers to a specific crystal structure of organic-inorganic semiconductor materials that have a composition notation  $ABX_3$  (Halide Perovskites) [6,7]. In this structure, the A site is occupied by an organic/inorganic cation, the B site by a metal cation, and the X site by a halide anion [8]. In PSCs, the A site consists of organic methylammonium ( $MA^+$ )  $CH_3NH_3^+$ , formamidinium ( $FA^+$ )  $CH_3N_2^+$ , or inorganic  $Cs^+$  and  $Rb^+$  or a mixture of these. The B site is occupied by  $Pb^{2+}$  or  $Sn^{2+}$ , and the X site is occupied by  $Cl^-$ ,  $Br^-$  or  $I^-$  or a mixture of them [9–11].

One of the main advantages of the perovskite material/film is its ease of fabrication via a solution process, making them scalable and low-cost [12]. PSCs have several main layers that are consistent across devices with some variations, such as the addition of a buffer layer. These main layers include a transparent conducting glass substrate, a hole transport layer (HTL) or a hole transport material (HTM), an electron transport layer (ETL) or an electron transport material (ETM), and the absorbing layer which is the perovskite active layer [1]. The architecture of the device significantly impacts the performance of PSCs and can be classified based on

\* Corresponding author.

E-mail address: [oalshehr@uwaterloo.ca](mailto:oalshehr@uwaterloo.ca) (O.D. Alshehri).

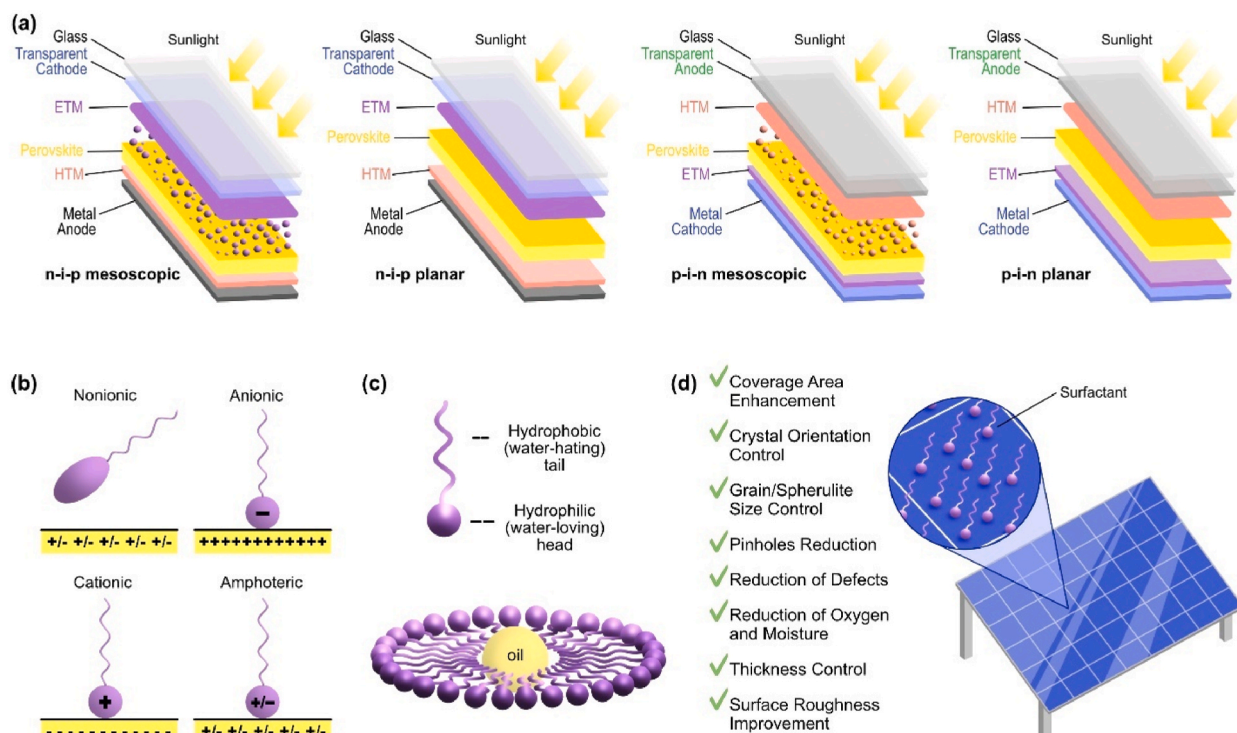


**Fig. 1.** (a) PCS layers of the four cell types. Note that there also exist ETL-free and HTL-free cells. (b) Different types of surfactants based on their charge. (c) Schematics illustrating the structure and function of a surfactant molecule. (d) A schematic of surfactant on PCS and their roles.

the transport layer facing the sunlight. The cell is categorized as either regular (n-i-p) or inverted (p-i-n) structure formation. Both types can further be classified as mesoscopic or planar structures; mesoscopic structures include a mesoporous layer, while planar structures contain only planar layers. Fig. 1 (a) illustrates the different PSC layers the four possible cell types (note that there are ETL-free and HTL-free structures [13]).

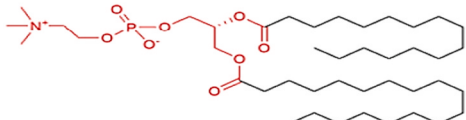
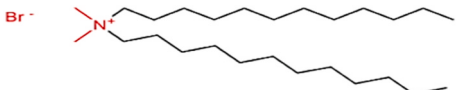
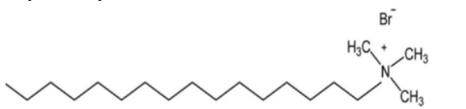
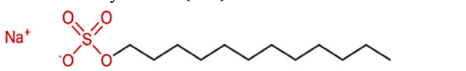
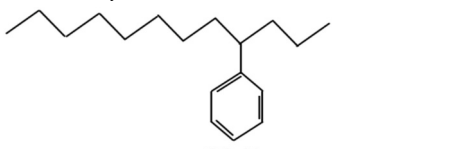
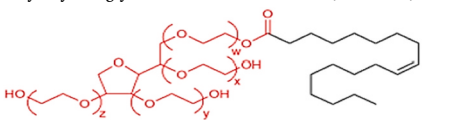
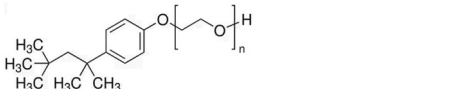
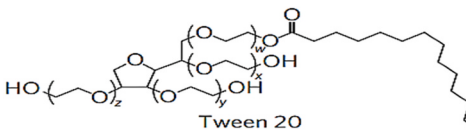
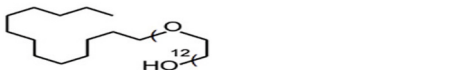
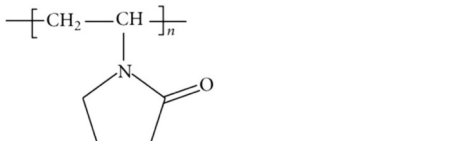
The power conversion efficiency (PCE) of PSCs has shown rapid improvement and a potential for further enhancement. However, compared to other types of solar cells, such as silicon, the stability of perovskite cells under real-life conditions is still insufficient [14]. This lack of stability is a major barrier to the commercialization of PSCs and it is considered the most challenging issue [15]. Several factors contribute to the instability of PSCs, including thermal effects (temperature), UV lights, hysteresis, burn-in degradation, moisture and oxygen, structural instability, interface defect, and field-induced degradation [16]. In addition, the presence of toxic components such as lead (Pb) makes PSCs less desirable commercially due to regulatory limitations [17,18]. Consequently, efforts have been made to develop lead-free PSCs as reported by Singh et al. [18], Sani et al. [19], and Babayigit et al. [20].

An important engineering enabler to PSCs is the additives during or post-cell fabrication [19–22]. Even in small amounts, these additives can significantly enhance cell performance. Surface-active agents, known as surfactants, are one such additive. Surfactants can be classified into anionic, cationic, amphoteric as illustrated in Fig. 1 (b) [23]. Anionic surfactants have a negatively charged hydrophilic head group [24] while cationic surfactants have a positively charged hydrophilic head group [25]. Amphoteric surfactants contain both negative and positive heads [26]. However, some surfactants like Silicone-based ones have unique properties including heat resistance and water repellency because of their silicone backbone [27]. Surfactants are organic molecules that reduce the interfacial tension between phases in a mixture, and promote mixing and dispersion [28]. They can form aggregates called *micelles* in aqueous solutions, where the hydrophobic tail acts as a shield from water and moisture, while the hydrophilic heads face the solvent. These heads and tails shown in Fig. 1 (c). This arrangement improves the adhesive properties of the surrounding solvent [29].

In this article, the various roles surfactants that they play in enhancing the performance PSCs will be discussed. How different surfactants impact key aspects of the PSCs will also be discussed, such as efficiency, coverage area, crystal orientation, grain size, and stability (see Fig. 1 (d)). To provide a comprehensive overview, all surfactants mentioned throughout the paper, along with their corresponding chemical structures, are listed in Table 1. This table serves as a detailed single reference for understanding the specific surfactants used so far and their chemical compositions, which will aid in the contextual understanding of their effects on PSCs performance. Note that there are three materials that are not surfactants but behave like surfactants which were included in this work: PE-PEG diblock copolymer, choline iodide, and choline chloride.

**Table 1**

Chemical structures and charge classification for different surfactants cited in this work. Note that three surfactant-like materials (behaving like surfactants) were discussed in this work, namely, PE-PEG diblock copolymer, choline iodide, and choline chloride.

Surfactant Type	Surfactants Name and Chemical Composition	Reference
Amphoteric	L- $\alpha$ -phosphatidylcholine (LP) 	[12]
Cationic	Didodecyltrimethylammonium bromide (DDAB)  Cetyltrimethylammonium bromide (CTAB) 	[12] [30]
Anionic	Sodium dodecyl sulfate (SDS)  Sodium dodecylbenzene sulfonate (SDBS) 	[12] [31]
Nonionic	Polyethylene glycol sorbitan monostearate (Tween 60)  Poly(ethylene glycol) (Triton X-100)  Polyoxyethylene (20) Sorbitan monolaurate (Tween 20)  Poly(ethylene glycol) tridecyl ether (PTE)  Polyvinyl pyrrolidone (PVP) 	[12] [9,32] [33,34] [35] [36]

## 2. Role in coverage area enhancement

The effectiveness of surfactants in PSCs is mainly due to their surface properties. During the blade coating process (one of the fabrication techniques to make PCSs), the perovskite solution tends to shrink quickly during the solution drying phase, which will in turn reduce the perovskite-covered area and, consequently, the light absorption.

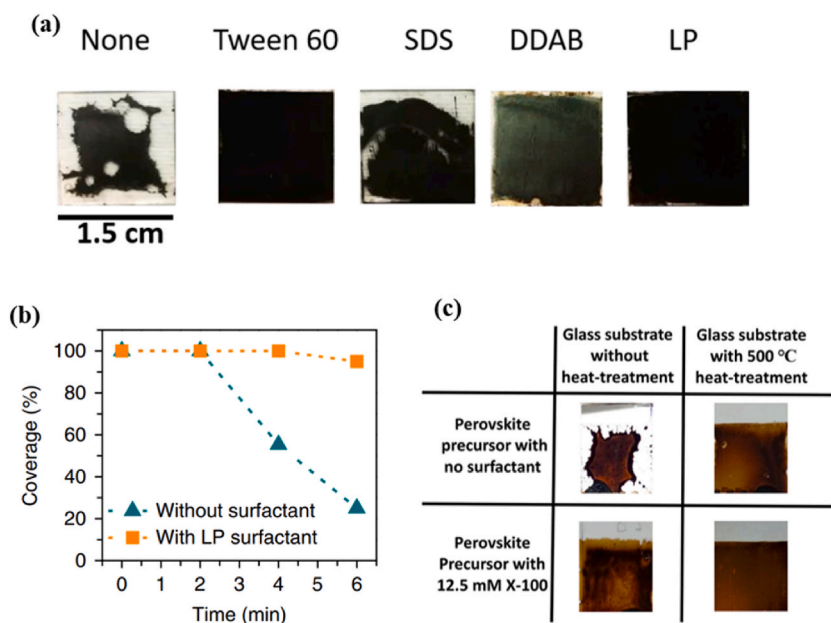


**Fig. 2.** (a) The perovskite film coverage from left to right: without any surfactant, with Tween 60, SDS, DDAB, and LP surfactants [12]. (b) Coverage % vs Evaporation Time for LP-assisted perovskite solution [12]. (c) The effect of adding the surfactant (Triton X-100) and the heat treatment on the coverage and uniformity of the perovskite film [9]. Used with permissions from Refs. [9,12].

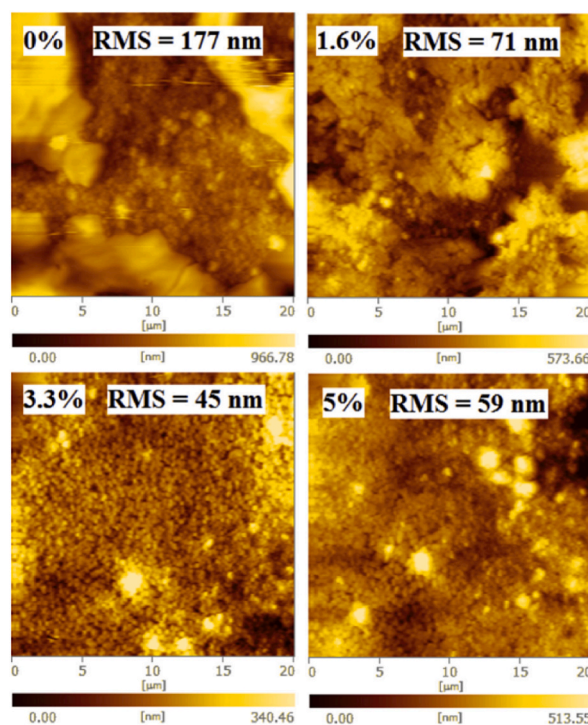


**Fig. 3.** The different samples using PVP gradually reveal the layer details. Used with permission from Ref. [38].

Huang et al. [12] used four surfactants to improve the coverage area of perovskite in PSC layers of ITO/PTAA/MAPbI<sub>3</sub>/fullerene (C60)/BCP/Cu; namely, amphoteric (LP), cationic (DDAB), non-ionic (Tween 60) and anionic (SDS) surfactants. Fig. 2 (a) shows the effect of these four surfactants on the 1.5 cm wide substrate and how surfactants improved the coverage area to nearly 100 % for Tween 60 and LP cases. This improvement is due to the hydrophilic nature induced by the surfactants, which pin the solution to the substrate

**Table 2**

Efficiencies of different samples using PVP surfactant. Used with permission from Ref. [38].

Sample	Efficiency (%)
Without PVP	4.51
1.6 % PVP	5.97
3.3 % PVP	8.74
5 % PVP	5.1

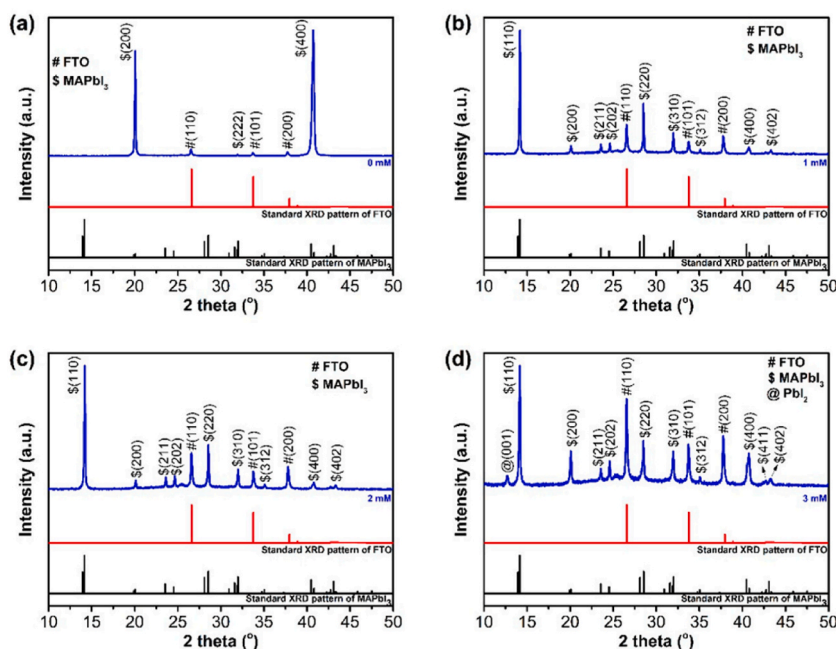


**Fig. 4.** Tween 20 surfactant effect on the preferred crystal orientation of the perovskite film without the surfactant addition as 0 mM (a) and with surfactant concentration of 1 mM (b), 2 mM (c), and 3 mM (d). Used with permission from Ref. [42].

and allow only vertical evaporation; hence, suppressing horizontal shrinkage. This phenomenon is known as the *pinning effect* [12,37]. LP was identified as the most effective surfactant in this case, and its relationship between coverage area and evaporation time was studied over a 6-min evaporation period, as shown in Fig. 2 (b).

Similarly, Taghavinia et al. [9] used Triton X-100 to enhance the coverage area of PSCs with layers composed of FTO/TiO<sub>2</sub> compact/TiO<sub>2</sub> mesoporous/Cs<sub>0.05</sub>[(MA<sub>0.17</sub>FA<sub>0.83</sub>)(Br<sub>0.17</sub>I<sub>0.83</sub>)<sub>3</sub>]<sub>0.95</sub> (note that the perovskite used is Cs<sub>0.05</sub>(MA<sub>0.17</sub>FA<sub>0.83</sub>)<sub>0.95</sub>). The surfactant was added in different concentrations (0.25, 1.75, and 12.5 mM) compared to a surfactant-free reference. The goal was to reduce the contact angle indicating lower surface energy, which implies greater surface wettability, hence better surface coverage. The best wettability (surface coverage) was achieved with a 12.5 mM concentration. Heat treatment further enhanced the coverage and uniformity of the film across the substrate as shown in Fig. 2 (c).

However, Zhao et al. [38] were the first to add (PVP) surfactants, a water-soluble polymer, during thin film formation, resulting in a 4.23 % increase in efficiency. PVP was added to the perovskite + TiO<sub>2</sub> solution (before coating) by 0–5 wt% relative to perovskite weight. As shown in Fig. 3, without surfactants (i.e. 0 %), obvious peaks cover the sides, which contain TiO<sub>2</sub> and an exposed area free of TiO<sub>2</sub>. As PVP weight increased, the area with TiO<sub>2</sub> covered more of the absorber film. At 3.3 wt%, full coverage was achieved, and at 5 wt% the coverage area became less uniform. The relationship between cell efficiency and coverage area enhancement is shown Table 2. PVP also improved crystallinity and reduced surface roughness [38,39].

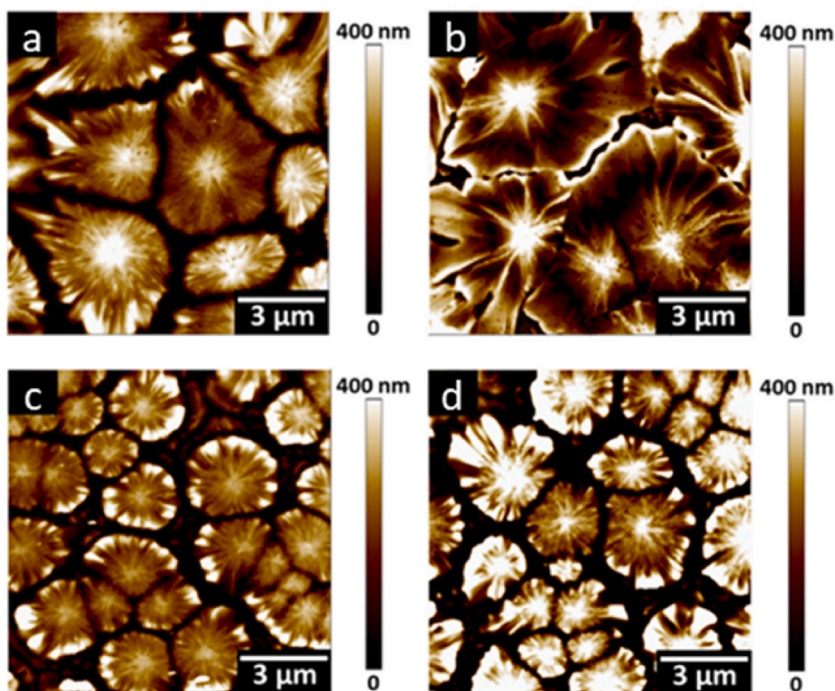
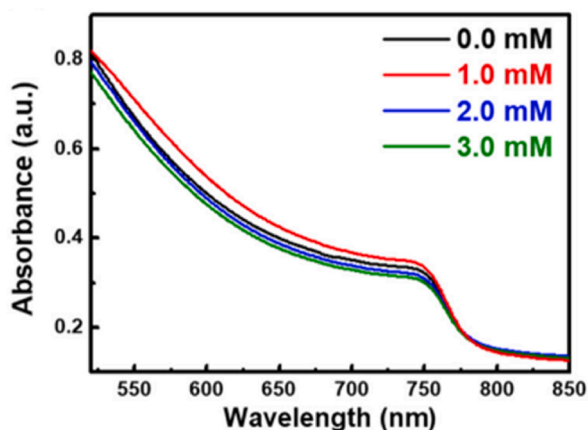
### 3. Role in crystal orientation

The transfer of holes and electrons at the interface of the absorption layer and charge transport layers (CTLs), which include the ETL and HTL, is influenced by the crystal plane. This can either enhance or reduce charge recombination. To study the effect of crystal orientation on photovoltaic properties, CH<sub>3</sub>NH<sub>3</sub>PbI<sub>3</sub> were fabricated by two different methods [40,41]. The first film was fabricated from CH<sub>3</sub>NH<sub>3</sub>I and PbI<sub>2</sub> (denoted by I<sub>3</sub>), and the second film was fabricated from CH<sub>3</sub>NH<sub>3</sub>Cl and PbI<sub>2</sub> (denoted by I<sub>2</sub>Cl). The efficiency was investigated using two types of cells architecture - planar and inverted. It was found that inverted cells made of I<sub>3</sub> show higher

**Table 3**

Different surfactant concentrations and their effect on spherulite size [42].

Tween 20 Concentration (mM)	Spherulite Size ( $\mu\text{m}$ )
0.0	4.0
1.0	6.0
2.0	<6.0
3.0	<6.0

**Fig. 5.** AFM images showing spherulite sizes for concentrations of 0.0 (a), 1.0 (b), 2.0 (c), and 3.0 mM (d). Used with permission from Ref. [42].**Fig. 6.** Effect of Tween 20 surfactant in wavelength absorbance of PSC. Used with permission from Ref. [42].

efficiency than those made of  $\text{I}_2\text{CI}$ ; an improvement attributed to the enhanced short-circuit current density ( $J_{\text{sc}}$ ) and fill factor (FF) of  $\text{I}_3$ . In contrast, planar cells made of  $\text{I}_2\text{CI}$  exhibited higher efficiency than those made of  $\text{I}_3$ . The difference in  $J_{\text{sc}}$  was assumed to be because of crystal orientation, where the layer conductivity significantly affects charge transfer between  $\text{CH}_3\text{NH}_3\text{PbI}_3$  and CTL.

In addition to cell architecture, the use of surfactants also affects the preferred crystal orientation. K.-M. Lee et al. [42] studied the

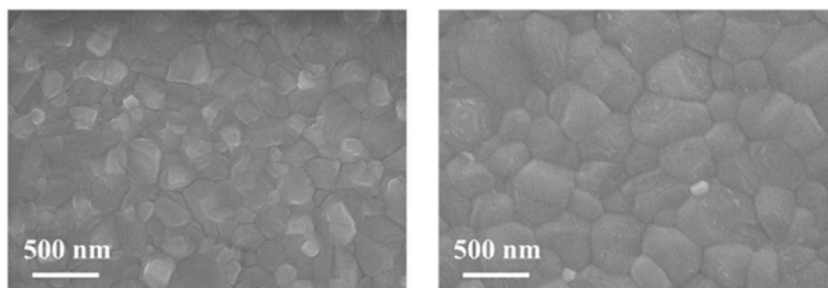


**Fig. 7.** SEM image showing a smaller grain size without using SDBS (left) and larger grains with using SDBS (right). Used with permission from Ref. [46].

**Table 4**

PCE with and without SDBS surfactant. Used with permission from Ref. [46].

Device	Scan	Efficiency (%)
Without SDBS	Forward	16.8
	Reverse	17.92
With SDBS	Forward	18.97
	Reverse	19.2

effect of surfactants on the device structure FTO/dense  $\text{TiO}_2$ /mesoporous  $\text{TiO}_2$ /MAPbI<sub>3</sub>/spiro-OMeTAD/Ag, as shown in Fig. 4. Without adding Tween 20 surfactant, the perovskite exhibits two peaks from the diffraction planes of (200) and (400). However, adding 1 mM of surfactant significantly reduces these peaks and changes the preferred crystal orientation of perovskite to the (110) and (220) planes, enhancing the material properties crucial for photovoltaic efficiency. This adjustment in crystal orientation, coupled with improved surface coverage and reduced defects, suggest that surfactants play a vital role in optimizing the fabrication and performance of perovskite solar cells.

#### 4. Role in grain/spherulite size control

In photovoltaics, increasing grain size has been identified as one of the key factors to enhance light absorbance [42]. This is because larger grain size significantly increase  $J_{sc}$  which ultimately determines the overall PCE of solar cells [43]. One way to achieve larger grain size is through rapid solvent evaporation. However, this often results in more gaps and grain boundaries, and this is where surfactants can positively contribute [12,42].

Lee et al. [42] investigated the effect of surfactants on a device with the following layer structure: FTO/dense  $\text{TiO}_2$ /mesoporous  $\text{TiO}_2$ /MAPbI<sub>3</sub>/spiro-OMeTAD/Ag. They used Tween 20 as the surfactant with different concentrations tested. The resulting spherulite sizes for various surfactant concentrations are shown in Table 3.

In addition to the increase in grain size, a reduction in grain boundaries was also observed, as shown by the AFM images in Fig. 5. Furthermore, a lower film-forming temperature was also achieved. The optimum temperature for thermal-assisted blade coating was previously found to be 130 °C [44,45], which dropped to 120 °C in this case due to the addition of 1 mM of Tween 20 surfactant.

These improvements were also reflected in the absorption spectra shown in Fig. 6, where maximum absorption was found for the 1 mM sample.

Similarly, Zhang et al. [46] showed that adding SDBS surfactant to the perovskite precursor solution results in larger grain sizes in the perovskite films. The coordination between SDBS and PbI<sub>2</sub> slows down the crystallization rate, allowing for the formation of high-quality perovskite films with more ordered grain growth.

Fig. 7 shows the difference between pristine MAPbI<sub>3</sub> film and the one with SDBS. The grain size is larger in the presence of SDBS, which benefits the properties of perovskite solar cells since larger grain sizes are associated with a reduction in grain boundaries and a lower density of defects in the perovskite film. Overall, Zhang et al. [46] highlighted the potential of surfactant engineering for enhanced grain size in perovskite solar cells, leading to improved stability and device performance, as shown in Table 4.

#### 5. Role in pinholes reduction

Because of its uniformity the perovskite film has fewer defects and greater grain sizes, which reduce the possibility of pinhole formation [47,48]. However, surfactants can help in further reducing these pinholes which are microscopic voids or gaps that occur between perovskite grains in the active layer of perovskite solar cells [49]. These voids can be considered as uncovered areas within the cell structure because they represent empty spaces between the hole transport layer (HTL) and the electron transport layer (ETL). Pinholes are detrimental to the performance of perovskite solar cells for several reasons. They can lead to direct physical contact between the HTL and ETL. This direct contact facilitates recombination of charge carriers (electrons and holes) without generating

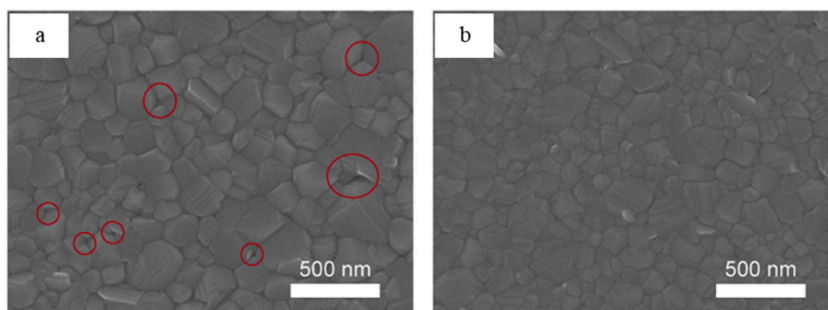


**Fig. 8.** SEM images showing the perovskite grains with pinholes before using the PTE surfactant (a) and after (b) and how it eliminated the pinholes. Used with permission from Ref. [35].

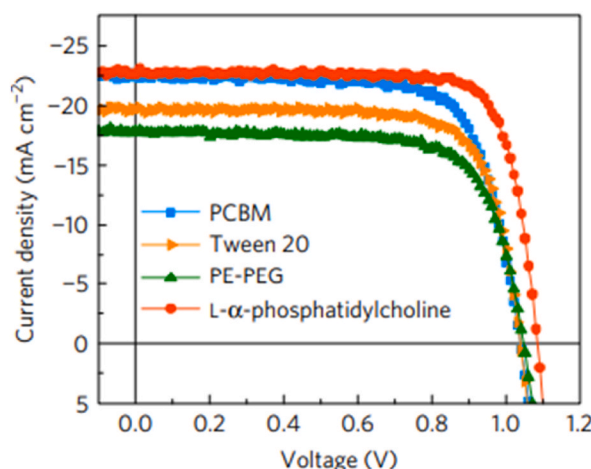


**Fig. 9.** J-V curves for the PSCs with different surfactants used. Used with permission from Ref. [33].

useful electric current, thereby reducing the overall efficiency of the solar cell. The presence of pinholes contributes to hysteresis in the current-voltage characteristics of perovskite solar cells which complicates the performance assessment and reduces the reliability of the cell's efficiency measurements [49]. Furthermore, pinholes act as pathways for current leakage, where the generated current bypasses the external circuit and reduces the amount of current that can be collected for useful power output. This leakage results in lower power conversion efficiency and poor device performance [12,50].

Pinholes, and inhomogeneities in general, result from localized evaporation and solidification, which can be reduced by stabilizing the ink during the coating process [47,51], which means altering the kinetics of crystallization of perovskite materials; something surfactants can do. For example, long-chain surfactants assist in controlling the precursor solution's drying dynamics, resulting in a more consistent crystallization process. Therefore, and to minimize the formation of pinholes and improve the quality of perovskite films, several deposition parameters such as spin coating speed, time, temperature, humidity, and annealing temperature must be carefully controlled [49]. In addition to optimizing deposition parameters, surfactants also influence the size and presence of pinholes. The kinetics of crystallization of perovskite materials can be changed by surfactants. Hwang et al. [35] studied the effect of PTE surfactant on a cell with the structure ITO/NiO<sub>x</sub>/MAPbI<sub>3</sub> - MAPbI<sub>3</sub>:PTE/PCBM/BCP/Ag. They found that using 0.07 wt% PTE surfactant could produce a pinhole-free perovskite film, as shown in Fig. 8.

## 6. Role in reduction of defects

Defects in perovskite solar cells, often formed during crystallization or annealing processes, can significantly impact efficiency [33, 35,52]. These defects, which have low formation energy, can easily form within the grains, at the grain boundaries and on the film's surface [53]. Reducing or passivating these defects is crucial for achieving highly efficient PSCs [54–56] where surfactants can play an important role in passivating defects. Zheng et al. [33] passivated PSCs composed of the following layers: ITO/PTAA (Poly(triarylamine))/perovskite/passivation layer/C<sub>60</sub>/bathocuproine (BCP)/copper (Cu). The passivation was achieved using the fullerene derivative (PCBM) phenyl-C61-butyric acid methyl ester and amphiphilic molecules such as LP, Tween 20, and PE-PEG to enhance moisture stability as an initial objective. As a result, the current density-voltage (J-V) curves of the MAPbI<sub>3</sub> perovskite material were enhanced, as shown in Fig. 9, with the best performance exhibited by the LP surfactant, which displayed hysteresis-free behavior.

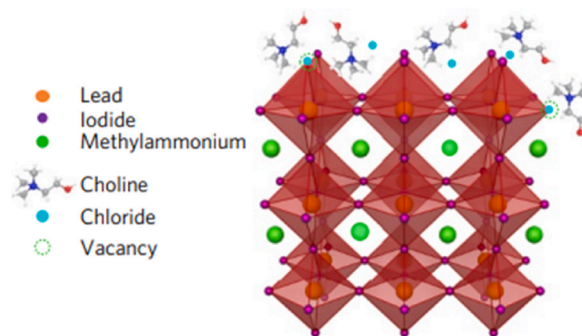


Fig. 10. Vacancies and their filler materials. Used with permission from Ref. [33].

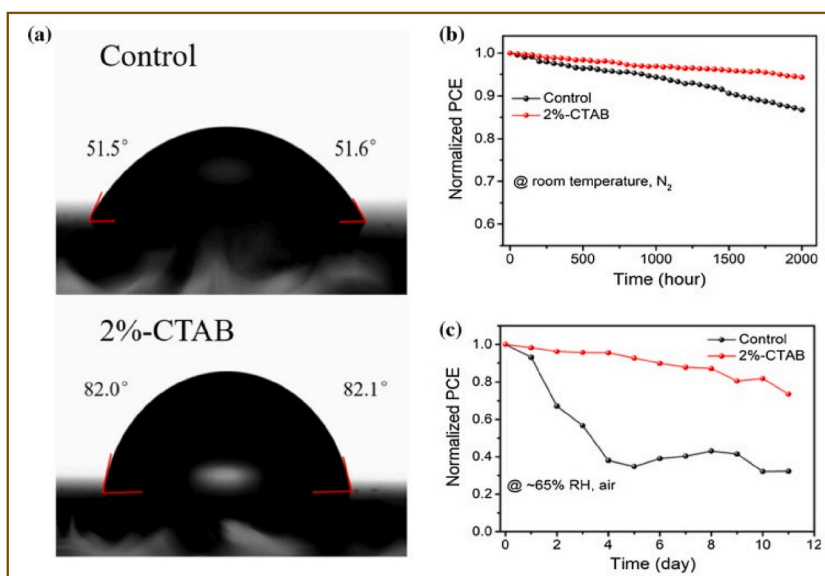


Fig. 11. (a) Contact angle without CTAB and with 2%- CTAB, (b) normalized PCE in room temperature and N<sub>2</sub>, (c) normalized PCE with 65 % relative humidity and air. Used with permission from Ref. [53].

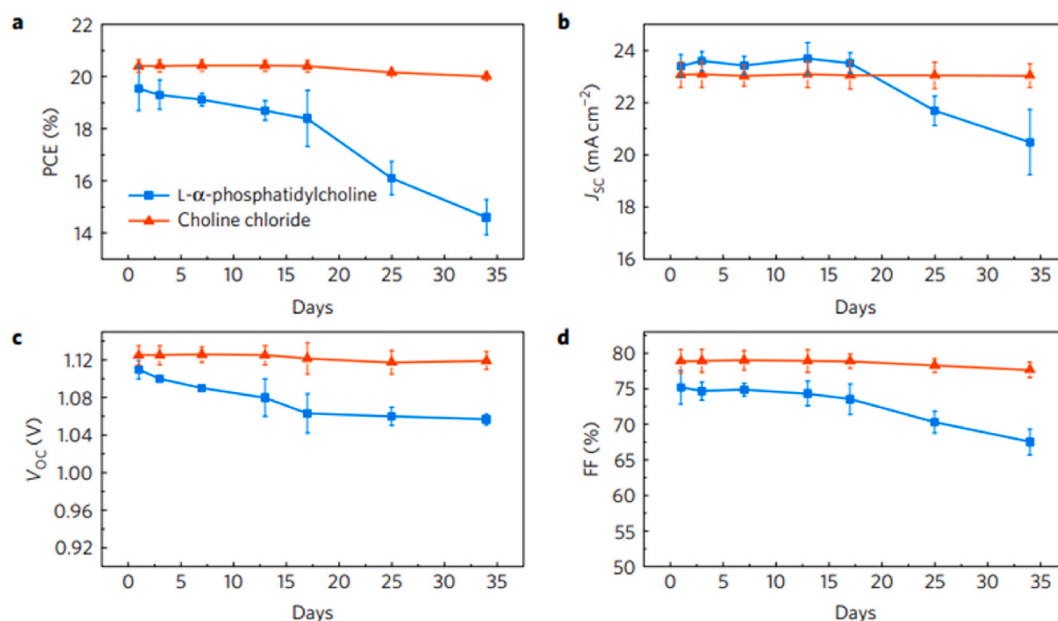
LP molecules passivate MAPbI<sub>3</sub> better than other surfactants due to their choline phosphate zwitterion structure, which means they have both positive and negative electrical charges. In contrast, other surfactants such as Tween 20 and PE-PEG have long alkyl chains [4,33]. This charge duality matches the cationic and anionic defects in MAPbI<sub>3</sub>, such as I<sup>-</sup> and MA<sup>+</sup> + vacancies. Quaternary ions are expected to occupy cuboctahedral sites to passivate MA<sup>+</sup> + vacancies on the film surfaces. Additionally, halide ions lost due to the evaporation of MAI during the thermal annealing process must be replaced by additional halide ions, as shown in Fig. 10.

Table 6 (at the end of the article) lists the power conversion efficiencies (PCEs) of different perovskite films along with their corresponding passivation layers.

## 7. Reduction of oxygen and moisture

While inorganic PSCs and lower-dimensional perovskite structures provide good protection from water, the organic cations in both organic and organic-inorganic hybrid PSCs tend to absorb moisture [46]. Water is a critical catalyst for the irreversible degradation of perovskite. For instance, in MAPbI<sub>3</sub>, both HI and MA are water-soluble [8]. Therefore, protecting the perovskite layer from direct contact is crucial for improving the stability of the PSCs [46]. Moisture's film degradation begins at the grain boundaries and surface defects [57]. One way to reduce moisture ingress is by increasing the contact angle with liquids, which will enhance the perovskite surface hydrophobicity and promote faster liquid wash-away [9].

Wang et al. [53] utilized CTAB surfactant to improve the stability of the PSCs with the layers of ITO/SnO<sub>2</sub>/Cs<sub>0.05</sub>(FA<sub>0.85</sub>MA<sub>0.1</sub>)Pb(I<sub>0.85</sub>Br<sub>0.15</sub>)<sub>3</sub>/spiro-OMeTAD/Ag. By subjecting PSCs with and without 2 % CTAB to a humidity control box at 65 % relative humidity, it was observed that PSCs with 2%-CTAB retained 73 % of their initial PCE, compared to only approximately 30 % retention without CTAB. This enhancement is attributed to the increased contact angle facilitated by the long alkyl chain of CTAB, imparting water



**Fig. 12.** Cell parameters with a blue line for LP surfactant and red for choline chloride, showing the PCE evolution in days (a), the current short circuit evolution in days (b), the voltage open circuit evolution in days (c), and the evolution of fill factor in days (d). Used with permission from Ref. [33].

resistance to the surface. While PCE improved up to 2 % CTAB, subsequent increments led to a decline in PCE, as depicted in Table 6 (lines 5–8). The contact angle of the droplet on the perovskite surface increased from 51.6° for the controlled sample to 82.1° for the 2%-CTAB sample (Fig. 11 (a)). Fig. 11(b) and (c), depict the normalized PCE over an 11-day period, showing that the 2%-CTAB sample maintained a PCE slightly above 0.7, while the control sample's PCE dropped to approximately 0.3. This difference emphasizes the positive impact of increasing hydrophobicity from CTAB addition on the efficiency of the PSCs.

However, Li et al. [33] investigated the impact of another surfactant, LP, in a device structure with ITO/PTAA/perovskite/passivation layer/C60/BCP/Cu. They observed that incorporating LP surfactant within the perovskite layer slowed moisture penetration, resulting in a 30 % reduction in PCE after 800 h of moisture exposure under ambient conditions. Fig. 12 illustrates the influence of LP surfactants on various cell parameters.

Their experiment demonstrates that the addition of LP surfactant improves the stability of PSCs with improvement in PCE,  $J_{sc}$ , open-circuit voltage ( $V_{oc}$ ), and FF. Additionally, Table 6 (lines 15 and 17) provides summary of the PCEs corresponding to different passivation layer concentrations.

## 8. Role in thickness control

Increasing or decreasing the thickness of the absorbing layer affects the optical properties of the perovskite solar cell either positively or negatively. A very thin absorber layer cannot absorb sufficient incident light, leading to a low photocurrent (known as short-circuit current) [58], whereas a very thick layer increases the reverse saturation current. Therefore, the functionality of the HTL depends on its thickness [59].

Overall, the HTL has two main functions: to transport photogenerated holes from the absorber layer to the electrode, and to prevent direct contact between the absorber layer and the electrode. The first function dictates avoiding a thicker HTL as it increases the distance between the absorber layer and the electrode. However, a thinner HTL should also be avoided since it may lead to unwanted interaction between the absorber layer and the electrode. For example, it has been shown that interaction between the perovskite's iodide ions and the electrode negatively affects device stability [7,60]. Therefore, a careful thickness trade-off must be sought. It was found that the optimum thickness of the absorber layer is in the range of 400–500 nm. Note that the absorber layer can be in the range of 100–1000 nm, with efficiency slowly increasing up to 600–700 nm beyond which no further advantage in efficiency is observed [7]. Surfactants have been found to be beneficial in achieving such thickness control.

Taghavinia et al. [9] utilized Triton X-100 surfactants in perovskite cells configuration FTO/TiO<sub>2</sub> compact/TiO<sub>2</sub> mesoporous/Cs<sub>0.05</sub>(MA<sub>0.17</sub>FA<sub>0.83</sub>) (Br<sub>0.17</sub>I<sub>0.83</sub>)<sub>3</sub>0.95/Spiro-OMeTAD/Au. Triton X-100 was added to investigate the effect of different concentrations on the contact angle by adding 0.25, 1.75 and 12.5 mM which caused more surface wettability manifested in the decrement of the contact angle from 22.2° to 20.1°, 19.2° and 18.6°, respectively. This improvement helps in getting better fluid flow of the perovskite precursor, leading to better film uniformity, which is consistent with Triton X-100 that is known in general to give better film quality [9]. Moreover, affecting the wetting properties of the precursor can be a control tool for the thickness of perovskite film [61], which is also constant with the results found in this work where both 0.8 and 1.5 M perovskite concentrations exhibited a correlation

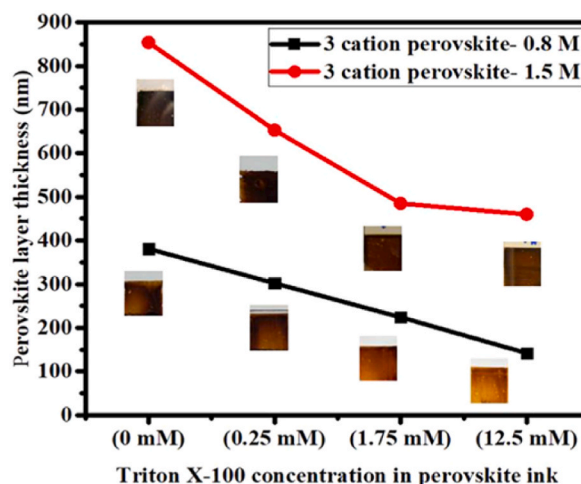


**Fig. 13.** Two perovskite layers thickness with different surfactant concentrations: 0 (without surfactant), 0.25, 1.75, 12.5 mM. A lighter color indicates a thinner film (i.e. thickness control). Used with permission from Ref. [9].

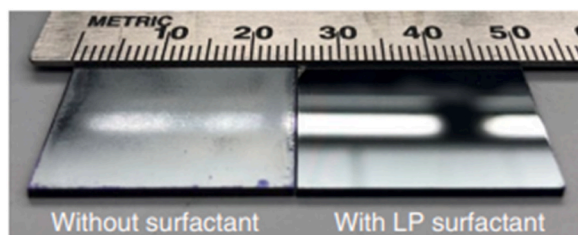


**Fig. 14.** Surfaces of PSC without using LP surfactant (left) and with usage of LP surfactant (right). Used with permission from Ref. [12].

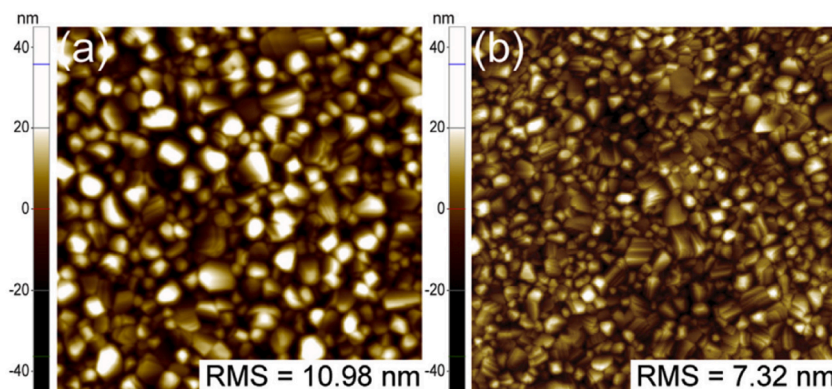


**Fig. 15.** RMS of sample surface without surfactant (left) and with surfactant (right). Used with permission from Ref. [35].

between increased surfactant concentration and a lighter perovskite film color. Such lighter coloring is an indication of a decrement in the film's thickness as influenced by the surfactant (see Fig. 13).

The thickness values for the 1.5 M perovskite concentration were closer to the optimal range compared to the 0.8 M concentration at similar surfactant concentrations. However, the 0.8 M concentration displayed better crystallinity at a surfactant concentration of 12.5 mM. The study found that increasing the blade-substrate gap and printing speed effectively increased thickness while preserving crystallinity. Hence, optimal parameters included a meniscus of 0.8 M perovskite mixed with 12.5 mM Triton X-100, printed with a 2 mm substrate-blade gap at a speed of 100 mm/min, resulting in a thickness of 487 nm.

**Table 5**

Summary of the article different types of surfactant and surface characteristics.

Surfactant	Surface properties
LP	Increases hydrophobicity and improves surface roughness.
DDAB	Enhance surface coverage area and better control of crystal orientation.
SDS	Enhance surface coverage area and improves surface roughness.
Tween 60	Enhance surface coverage area and control film thickness.
Triton X-100	Enhance surface coverage area, reduce roughness and control film thickness.
PVP	Enhance surface coverage area, reduce roughness and control of crystal orientation.
SDBS	Enhance surface coverage area, larger grain size and reduces grain boundaries.
CTAB	Increases hydrophobicity and improves surface roughness.
Tween 20	Improves surface roughness, control of crystal orientation and better film uniformity.
PTE	Reduce pinholes and improves surface roughness.

**Table 6**

Summary of the article containing different perovskite materials, surfactants used, coating techniques, and different performance indicators.

N	Perovskite composition	layer	Coating technique	Surfactant	Others	V <sub>OC</sub> (V)	J <sub>SC</sub> (mA cm <sup>-2</sup> )	FF (%)	PCE (%)	ref
1	MAPbI <sub>3</sub>	With Absorber layer	Blade-coating	LP (0.25)	-	1.07	19.5	72.1	15.0	[12]
2						1.06	19.0	70.5	14.2	
3						1.07	20.3	68.9	15.0	
4						1.06	20.2	66.1	14.2	
5	CS <sub>0.05</sub> (FA <sub>0.85</sub> MA <sub>0.1</sub> )Pb		Spin-coating	w/o CTAB		1.072	22.76	74.3	18.13	[53]
6	(I <sub>0.85</sub> Br <sub>0.15</sub> ) <sub>3</sub>			1 % CTAB		1.090	23.35	75.1	19.18	
7				2 % CTAB		1.114	23.32	79.1	20.54	
8				3 % CTAB		1.059	22.71	72.4	17.41	
9	MAPbI <sub>3</sub>	Under Absorber layer		w/o SDBS		1.060	21.06	72.84	16.26	[51]
10				SDBS (0.05)		1.090	22.94	75.67	18.73	
11				SDBS (0.2)		1.124	22.94	78.19	20.15	
12				SDBS (1)		1.111	22.55	77.24	19.35	
13		Above (or after) Absorber layer		SDBS (10)		1.077	21.39	73.83	17.01	[33]
14				-	PCBM	1.06	22.89	75.05	18.2	
15				LP	-	1.08	22.7	80.0	19.6	
16				-	PCBM	1.04	22.5	73	17.1	
17					Choline chloride	1.15	22.9	76	20	
18	FA <sub>0.85</sub> MA <sub>0.15</sub> Pb				PCBM	1.03	23.7	79	19.2	
19	(I <sub>0.85</sub> Br <sub>0.15</sub> ) <sub>3</sub>				Choline chloride	1.14	23.7	78	21	
20	FA <sub>0.83</sub> MA <sub>0.17</sub> Pb				PCBM	1.12	17.1	66	12.6	
21	(I <sub>0.6</sub> Br <sub>0.4</sub> ) <sub>3</sub>				Choline chloride	1.15	19.4	77	17.2	
18	CS <sub>0.05</sub> [(MA <sub>0.17</sub> FA <sub>0.83</sub> )(Br <sub>0.17</sub> I <sub>0.83</sub> ) <sub>3</sub> ]I <sub>0.95</sub>	With Absorber layer		Triton X-100 (0)	-	1.05	19.23	0.68	11.2 ± 0.9	[9]
19				Triton X-100 (0.25)		1.05	19.15	0.67	11.5 ± 0.4	
20				Triton X-100 (1.75)		1.04	19.12	0.69	14.0 ± 0.3	
21				Triton X-100 (12.5)		1.04	23.98	0.67	15.1 ± 0.3	
22				Triton X-100 (12.5)		1.04	21.06	0.66	12.3 ± 0.4	
23	MAPbI <sub>3</sub>			Without PTE	-	-	-	-	15.17 forward	[35]
24									15.6 reverse	
25				PTE (0.07 wt %)					16.32 forward	
26									16.96 reverse	
27			Thermal-assisted blade coating	Without	-	1.022 ± 0.020	19.89 ± 0.87	67.8 ± 1.7	13.79 ± 0.82	[42]
28				Tween 20		1.035 ± 0.022	21.46 ± 0.46	70.9 ± 1.2	15.75 ± 0.62	
29				Tween 20		1.022 ± 0.025	21.02 ± 0.27	69.5 ± 2.9	15.45 ± 0.75	
30				Tween 20		1.046 ± 0.023	20.03 ± 1.18	69.6 ± 0.7	14.59 ± 0.96	

**Table 7**  
Chemical type of surfactants used.

Surfactant	Type
LP (L- $\alpha$ -phosphatidylcholine)	Amphoteric surfactant
DDAB (Didodecyltrimethylammonium bromide)	Cationic surfactant
SDS (Sodium dodecyl sulfate)	Anionic surfactant
Tween 60 (Polyethylene glycol sorbitan monostearate)	Non-ionic surfactant
Triton X-100 (poly(ethylene glycol))	Non-ionic surfactant
PE-PEG diblock copolymer	Amphiphilic molecule
Choline chloride	Quaternary ammonium salt
Choline iodide	Quaternary ammonium salt
Tween 20 (Polyoxyethylene (20) Sorbitan monolaurate)	Non-ionic surfactant
PTE (poly(ethylene glycol) tridecyl ether)	Non-ionic surfactant
PVP (polyvinyl pyrrolidone)	Non-ionic surfactant
SDBS (sodium dodecylbenzene sulfonate)	Anionic surfactant
CTAB (Cetyltrimethylammonium bromide)	Cationic surfactant

## 9. Role in surface roughness improvement

The surface roughness of perovskite films significantly affects their performance. A rough surface can lead to defects and increased recombination losses which ultimately lowers the efficiency of the solar cells. Surfactants can minimize film roughness by enhancing the wetting properties and controlling the morphology of the perovskite layer which will in turn improve the contact with the HTL [46]. Huang et al. [12] investigated roughness improvement in a device with layers ITO/PTAA/MAPbI<sub>3</sub>/C<sub>60</sub>/BCP/Cu, using LP surfactant. Usage of the surfactant resulted in a notably smoother perovskite film compared to the non-surfactant film, as evidenced by a significantly lower root-mean-square (RMS) roughness. The RMS roughness for the surfactant-assisted film is 14.5 nm compared to the no-surfactant film of 167.7 nm as shown in Fig. 14.

Similarly, Hwang et al. [35] employed another surfactant (PTE) to enhance the roughness of a PSC device, demonstrating a reduction in surface film roughness with the addition of PTE. They observed that adding small amount of PTE (0.07 wt%) can reduce the RMS value of the surface roughness from 10.98 nm to 7.32 nm as shown in Fig. 15.

Furthermore, Wang et al. [53] utilized CTAB surfactant to improve the roughness of perovskite solar cells, reporting a decrease in RMS values (15.9 nm–9.38 nm) with the addition of 2 % CTAB, as reflected in the efficiency improvement.

## 10. Summary and outlook

Perovskite solar cells (PSCs) have rapidly advanced, reaching an efficiency of 26.1 % in about ten years of time. This remarkable progress has initiated significant research interest, primarily due to the ease of fabrication and low cost associated with perovskite materials. When surfactants are added to perovskite cells it can greatly impact different surface characteristics and enhance the quality of the film and performance of the devices. Surfactants can also enhance surface coverage and crystal alignment which play a role in creating uniform films and improving efficient charge transport. Moreover, surfactants give the capability to manage the size of grains, minimize imperfections and controlling the thickness of the film. These factors can individually and collectively enhance the performance of solar cells. The effect of all surfactants mentioned in paper in surface characteristics is listed in Table 5. Moreover, Table 6 provides a detailed overview, outlined different perovskite materials, surfactants utilized, coating techniques employed, and different performance indicators. In addition, Table 7 (in addition to Table 1) illustrate the chemical structures of the cited chemical compounds and corresponding surfactants for reference.

Despite the above advantages, PSCs face some challenges, particularly in terms of stability and the presence of toxic materials like lead, where surfactants had shown to be a potential venue for addressing such challenges. More surfactants can be explored in this venue, in addition to the ones explore so far. A good inspiration source/guide could be the surfactants used in other solar cell types, especially the polymer solar cells since it is the closest to the perovskites in terms of the nature of materials. Some surfactants used there has been already explored for perovskite which are PTE [62–64] DDAB [65], and SDS [66]. However, different surfactants not used with perovskites were used in polymer solar cells and they showed great potential like increasing the cell's power conversion efficiency in one case from 8.69 % to 17.04 % using surfactant encapsulated polyoxometalate complex [(C<sub>8</sub>H<sub>17</sub>)<sub>4</sub>N]<sub>4</sub>[SiW<sub>12</sub>O<sub>40</sub>] (TOASiW<sub>12</sub>) as reported by Qiu et al. [67]. Such surfactants include PCBTE [68], polyethylenimine (PEI) [69], PEG-TmDD (polyethylene glycol 2,5,8,11-tetramethyl-6-dodecyl-5,8-diol) [70], Surfynol 104 PA [71], Surfynol 104 EG [71], FS-31 [72], oleamide [73], dodecylsulfate (DS<sup>−</sup>) [74], cetylpyridinium bromide (CPB) [75], and BYK-333 [76]. However, some surfactants used in polymer solar cells were used after being mixed with other materials such as zinc oxide bonded with 1 surfactant (1-ZnO) where 1 is the short name for the surfactant molecule (E)-2-cyano-3-(5'-(4-(dibutylamino)styryl)-2,2'-bithiophen-5-yl)acrylic acid. Moreover, other surfactants were mixed with nano-carbons such the bis-adduct fullerene surfactant (C<sub>60</sub>-bis) [77], the DDAB surfactant which was mixed with graphene oxide (GO) sheets then both get mixed with the active PV layer [65], and the 3D surfactant-based graphene composite in PM6:Y6-based polymer solar cells as cathode interfacial materials (the 3D surfactants were based on POSSFN (1,3,5,7,9,11,13,15-octa-(9-bis(30-(N,N-dimethylamino)pro-pyl)-2,7-fluorene)-vinylpentacyclo-octasiloxane) and ADMAFN (1,3,5,7-tetra-(9-bis(30-(N,N-dimethylamino)propyl)-2,7-fluorene)-adamantane) [78]. In case of using graphene, the resultant improvement in cell's conductivity could be attributed to the surfactants' large adsorption energies on graphene [78]. This graphene-based improvements for

perovskite solar cells has been discussed in a recent review by Znidi et al. [79], yet to the best of our knowledge, graphene-enhanced surfactants have not been fully explored in perovskite solar cells, which is something we recommend. Note that graphene-enhanced surfactants has been utilized also for other solar cell types like the silicon solar cells as studied by Muramoto et al. [80], De Nicola et al. [81], Yu et al. [82], Arena et al. [83], and Wei et al. [84].

## Funding sources

This work is funded and supported by Natural Sciences and Engineering Research Council of Canada (NSERC) and Mitacs (from Prof. Ban).

## CRediT authorship contribution statement

**Abdullah Alasiri:** Writing – original draft. **Khalid Zubair:** Project administration, Investigation. **Shazzad Rassel:** Writing – review & editing. **Dayan Ban:** Funding acquisition, Writing – review & editing. **Omar D. Alshehri:** Writing – review & editing, Supervision, Conceptualization.

## Declaration of competing interest

The authors declare the following financial interests/personal relationships which may be considered as potential competing interests: Dayan Ban reports financial support was provided by Natural Sciences and Engineering Research Council of Canada. Dayan Ban reports financial support was provided by Mitacs Canada. If there are other authors, they declare that they have no known competing financial interests or personal relationships that could have appeared to influence the work reported in this paper.

## Acknowledgment

The authors would like to thank Owen Gibbs, from the University of Waterloo's Nanotechnology Engineering undergraduate program for his proof reading of this manuscript.

## Acronyms

PSCs	Perovskite solar cells
PVs	Photovoltaic devices
HTM	Hole transport material
HTL	Hole transport layer
ETM	Electron transport material
ETL	Electron transport layer
n - i - p	Regular structure formation
p-i - n	Inverted structure formation
PCE	Power conversion efficiency
LP	L- $\alpha$ -phosphatidylcholine
DDAB	Didodecyldimethylammonium bromide
SDS	Sodium dodecyl sulfate
Tween 60	Polyethylene glycol sorbitan monostearate
Triton X-100	Poly(ethylene glycol)
Tween 20	Polyoxyethylene (20) Sorbitan monolaurate
PTE	Poly(ethylene glycol) tridecyl ether
PVP	Polyvinyl pyrrolidone
SDBS	Sodium dodecylbenzene sulfonate
CTAB	Cetyltrimethylammonium bromide
C60	Fullerene
CTLs	Charge transport layers
GBs	Grain boundaries
BCP	Bathocuproine
Cu	Copper
RMS	Root-mean-square
PCBM	Phenyl-C61-butyrac acid methyl ester

## References

- [1] J.-P. Correa-Baena, et al., Promises and challenges of perovskite solar cells, *Science* 358 (6364) (2017) 739–744.
- [2] V. Gonzalez-Pedro, et al., General working principles of CH<sub>3</sub>NH<sub>3</sub>PbX<sub>3</sub> perovskite solar cells, *Nano Lett.* 14 (2) (2014) 888–893.
- [3] D. McPhee, Researchers take a step closer to better, more affordable solar cells, [Research News] 2024 (Apr 11, 2024) [cited 2024 30 Aug, <https://www.mccormick.northwestern.edu/news/articles/2024/04/researchers-take-a-step-closer-to-better-more-affordable-solar-cells/>].
- [4] Best Research-Cell Efficiency Chart. [cited 2022 12/7/2022], NREL maintains a chart of the highest confirmed conversion efficiencies for research cells for a range of photovoltaic technologies, plotted from 1976 to the present.]. <https://www.nrel.gov/pv/cell-efficiency.html>.
- [5] M. Nakamura, et al., Cd-free Cu (In, Ga)(Se, S) 2 thin-film solar cell with record efficiency of 23.35%, *IEEE J. Photovoltaics* 9 (6) (2019) 1863–1867.
- [6] N.-G. Park, Perovskite solar cells: an emerging photovoltaic technology, *Mater. Today* 18 (2) (2015) 65–72.
- [7] A. Bag, et al., Effect of absorber layer, hole transport layer thicknesses, and its doping density on the performance of perovskite solar cells by device simulation, *Sol. Energy* 196 (2020) 177–182.
- [8] D. Wang, et al., Stability of perovskite solar cells, *Sol. Energy Mater. Sol. Cell.* 147 (2016) 255–275.
- [9] E. Parvazian, et al., Photovoltaic performance improvement in vacuum-assisted meniscus printed triple-cation mixed-halide perovskite films by surfactant engineering, *ACS Appl. Energy Mater.* 2 (9) (2019) 6209–6217.
- [10] F. Bella, et al., Caesium for perovskite solar cells: an overview, *Chem.-Eur. J.* 24 (47) (2018) 12183–12205.
- [11] Y. Zhang, et al., An MBene modulating the buried SnO<sub>2</sub>/perovskite interface in perovskite solar cells, *Angew. Chem. Int. Ed.* 63 (27) (2024) e202404385.
- [12] Y. Deng, et al., Surfactant-controlled ink drying enables high-speed deposition of perovskite films for efficient photovoltaic modules, *Nat. Energy* 3 (7) (2018) 560–566.
- [13] I. Hussain, et al., Functional materials, device architecture, and flexibility of perovskite solar cell, *Emergent Materials* 1 (3) (2018) 133–154.
- [14] T.A. Berhe, et al., Organometal halide perovskite solar cells: degradation and stability, *Energy Environ. Sci.* 9 (2) (2016) 323–356.
- [15] R. Wang, et al., A review of perovskites solar cell stability, *Adv. Funct. Mater.* 29 (47) (2019) 1808843.
- [16] S.S. Dipta, A. Uddin, Stability issues of perovskite solar cells: a critical review, *Energy Technol.* 9 (11) (2021) 2100560.
- [17] G. Rodriguez-Garcia, et al., Toxicity assessment of lead and other metals used in perovskite solar panels. 2022 IEEE 49th Photovoltaics Specialists Conference (PVSC), IEEE, 2022.
- [18] Z. Guo, B. Lin, Machine learning stability and band gap of lead-free halide double perovskite materials for perovskite solar cells, *Sol. Energy* 228 (2021) 689–699.
- [19] H. Bi, et al., Double side passivation of phenylethyl ammonium iodide for all perovskite tandem solar cell with efficiency of 26.8%, *Eco Energy* 2 (3) (2024) 337–502.
- [20] C. Zuo, et al., Natural drying yields efficient perovskite solar cells, *DeCarbon* 2 (2023) 100020.
- [21] H. Zhang, N.-G. Park, Progress and issues in p-i-n type perovskite solar cells, *DeCarbon* 3 (2024) 100025.
- [22] L. Zhang, et al., Major strategies for improving the performance of perovskite solar cells, *iEnergy* 2 (3) (2023) 172–199.
- [23] M.R. Porter, *Handbook of Surfactants*, Springer, 2013.
- [24] G. von Maltzahn, et al., Positively charged surfactant-like peptides self-assemble into nanostructures, *Langmuir* 19 (10) (2003) 4332–4337.
- [25] G. Para, et al., Surface activity of cationic surfactants, influence of molecular structure, *Colloids Surf. A Physicochem. Eng. Asp.* 365 (1–3) (2010) 215–221.
- [26] R. Sarkar, et al., Properties and applications of amphoteric surfactant: a concise review, *J. Surfactants Deterg.* 24 (5) (2021) 709–730.
- [27] L.J. Petroff, S.A. Snow, *Silicone Surfactants*. *Silicone Surface Science*, 2012, pp. 243–280.
- [28] D. Brown, Introduction to surfactant biodegradation, in: *Biodegradability of Surfactants*, Springer, 1995, pp. 1–27.
- [29] M.J. Rosen, J.T. Kunjappu. *Surfactants and Interfacial Phenomena*, John Wiley & Sons, 2012.
- [30] Z. Chiang, et al., Experimental investigation and performance evaluation of modified viscoelastic surfactant (VES) as a new thickening fracturing fluid, *Polymers* 12 (7) (2020) 1470.
- [31] M.A. Saleemi, et al., Elucidation of antimicrobial activity of non-covalently dispersed carbon nanotubes, *Materials* 13 (7) (2020) 1676.
- [32] National Center for Biotechnology Information, 2022 [cited 2022 12/12].
- [33] X. Zheng, et al., Defect passivation in hybrid perovskite solar cells using quaternary ammonium halide anions and cations, *Nat. Energy* 2 (7) (2017) 1–9.
- [34] G. Wypych, *Databook of Antistatics*, Elsevier, 2013.
- [35] J. Hong, H. Kim, I. Hwang, Defect site engineering for charge recombination and stability via polymer surfactant incorporation with an ultra-small amount in perovskite solar cells, *Org. Electron.* 73 (2019) 87–93.
- [36] K. Sreekanth, et al., Optical and electrical conductivity studies of VO<sub>2</sub><sup>+</sup> doped polyvinyl pyrrolidone (PVP) polymer electrolytes, *J. Sci.: Advanced Materials and Devices* 4 (2) (2019) 230–236.
- [37] M.L. McLauchlin, et al., Evaporative properties and pinning strength of laser-ablated, hydrophilic sites on lotus-leaf-like, nanostructured surfaces, *Langmuir* 23 (9) (2007) 4871–4877.
- [38] Y. Ding, et al., Surfactant enhanced surface coverage of CH<sub>3</sub>NH<sub>3</sub>PbI<sub>3</sub>–xCl<sub>x</sub> perovskite for highly efficient mesoscopic solar cells, *J. Power Sources* 272 (2014) 351–355.
- [39] C. Zuo, L. Ding, Drop-casting to make efficient perovskite solar cells under high humidity, *Angew. Chem. Int. Ed. Engl.* 60 (20) (2021) 11242–11246.
- [40] S. Bae, et al., CH<sub>3</sub>NH<sub>3</sub>PbI<sub>3</sub> crystal orientation and photovoltaic performance of planar heterojunction perovskite solar cells, *Sol. Energy Mater. Sol. Cell.* 160 (2017) 77–84.
- [41] J. Yin, et al., Interfacial charge transfer anisotropy in polycrystalline lead iodide perovskite films, *J. Phys. Chem. Lett.* 6 (8) (2015) 1396–1402.
- [42] K.-M. Lee, et al., Surfactant Tween 20 controlled perovskite film fabricated by thermal blade coating for efficient perovskite solar cells, *Nanomaterials* 12 (15) (2022) 2651.
- [43] M.K. Kim, et al., Effective control of crystal grain size in CH<sub>3</sub>NH<sub>3</sub>PbI<sub>3</sub> perovskite solar cells with a pseudohalide Pb (SCN)<sub>2</sub> additive, *CrystEngComm* 18 (32) (2016) 6090–6095.
- [44] K.-M. Lee, et al., Thermal assisted blade coating methylammonium lead iodide films with non-toxic solvent precursors for efficient perovskite solar cells and sub-module, *Sol. Energy* 204 (2020) 337–345.
- [45] K.-M. Lee, et al., High-performance perovskite solar cells based on dopant-free hole-transporting material fabricated by a thermal-assisted blade-coating method with efficiency exceeding 21%, *Chem. Eng. J.* 427 (2022) 131609.
- [46] W. Zhang, et al., Surfactant sodium dodecyl benzene sulfonate improves the efficiency and stability of air-processed perovskite solar cells with negligible hysteresis, *Sol. RRL* 4 (11) (2020) 2000376.
- [47] L. Wang, et al., Surfactant engineering for perovskite solar cells and submodules, *Matter* 6 (9) (2023) 2987–3005.
- [48] Y. Ren, et al., Long-chain gemini surfactant-assisted blade coating enables large-area carbon-based perovskite solar modules with record performance, *Nano-Micro Lett.* 15 (1) (2023) 182.
- [49] A. Bahtiar, S. Rahmanita, Y. Inayat, Pin-hole free perovskite film for solar cells application prepared by controlled two-step spin-coating method, in: *IOP Conference Series: Materials Science and Engineering*, IOP Publishing, 2017.
- [50] B.-E. Cohen, et al., Impact of antisolvent treatment on carrier density in efficient hole-conductor-free perovskite-based solar cells, *J. Phys. Chem. C* 120 (1) (2016) 142–147.
- [51] T. Wang, et al., High efficiency perovskite solar cells with tailorable surface wettability by surfactant, *J. Power Sources* 448 (2020) 227584.
- [52] Y. Sun, et al., Regulate defects and energy levels for perovskite solar cells by co-modification strategy, *Nano Energy* 121 (2024) 109245.
- [53] Q. Wang, et al., Multifunctional molecules of surfactant to support enhanced efficiency and stability for perovskite solar cells, *J. Mater. Sci.* 55 (30) (2020) 14761–14772.
- [54] H. Cao, et al., Reducing defects in perovskite solar cells with white light illumination-assisted synthesis, *ACS Energy Lett.* 4 (12) (2019) 2821–2829.

- [55] Y. Lao, et al., Efficient perovskite solar cells with enhanced thermal stability by sulfide treatment, *ACS Appl. Mater. Interfaces* 14 (23) (2022) 27427–27434.
- [56] Z. Liu, et al., Biomaterial improves the stability of perovskite solar cells by passivating defects and inhibiting ion migration, *ACS Appl. Mater. Interfaces* 16 (24) (2024) 31218–31227.
- [57] M. Jung, et al., Structural features and their functions in surfactant-armoured methylammonium lead iodide perovskites for highly efficient and stable solar cells, *Energy Environ. Sci.* 11 (8) (2018) 2188–2197.
- [58] J. García, et al., Photovoltaic and fuel cells in power microelectromechanical systems for smart energy management, in: *Smart Sensors and MEMs.*, Elsevier, 2018, pp. 461–498.
- [59] T. Ouslimane, et al., Impact of absorber layer thickness, defect density, and operating temperature on the performance of MAPbI<sub>3</sub> solar cells based on ZnO electron transporting material, *Heliyon* 7 (3) (2021) e06379.
- [60] G.-W. Kim, D.V. Shinde, T. Park, Thickness of the hole transport layer in perovskite solar cells: performance versus reproducibility, *RSC Adv.* 5 (120) (2015) 99356–99360.
- [61] Z. Yuan, et al., Approximately 800-nm-thick pinhole-free perovskite films via facile solvent retarding process for efficient planar solar cells, *ACS Appl. Mater. Interfaces* 8 (50) (2016) 34446–34454.
- [62] B. Park, Y.H. Huh, M. Kim, Surfactant additives for improved photovoltaic effect of polymer solar cells, *J. Mater. Chem.* 20 (48) (2010) 10862–10868.
- [63] B. Park, J.C. Shin, Y.H. Huh, Interface-engineering additives for inverted BHJ polymer solar cells, *Sol. Energy Mater. Sol. Cells* 110 (2013) 15–23.
- [64] Y.H. Huh, B. Park, Interface-engineering additives of poly(oxyethylene tridecyl ether) for low-band gap polymer solar cells consisting of PCDTBT: PCBM70 bulk-heterojunction layers, *Opt Express* 21 (S1) (2013) A146–A156.
- [65] Y. Wang, et al., The role of surfactant-treated graphene oxide in polymer solar cells: mobility study, *Org. Electron.* 53 (2018) 303–307.
- [66] Y.M. Chang, et al., Electrostatic self-assembly conjugated polyelectrolyte-surfactant complex as an interlayer for high performance polymer solar cells, *Adv. Funct. Mater.* 22 (15) (2012) 3284–3289.
- [67] J. Qiu, et al., Surfactant-encapsulated polyoxometalate complex as a cathode interlayer for nonfullerene polymer solar cells, *CCS Chem.* 4 (3) (2022) 975–986.
- [68] Y.-C. Lai, et al., Enhancement of power conversion efficiency and long-term stability of P3HT/PCBM solar cells using C60 derivatives with thiophene units as surfactants, *Sol. Energy Mater. Sol. Cells* 97 (2012) 164–170.
- [69] J.-J. Dong, et al., Synthesis of ZnO nanocrystals and application in inverted polymer solar cells, *Nanoscale Res. Lett.* 12 (2017) 1–5.
- [70] Z. Li, et al., A nonionic surfactant simultaneously enhancing wetting property and electrical conductivity of PEDOT: PSS for vacuum-free organic solar cells, *Sol. Energy Mater. Sol. Cell.* 137 (2015) 311–318.
- [71] S.W. Heo, et al., Enhanced performance in inverted polymer solar cells via solution process: morphology controlling of PEDOT: PSS as anode buffer layer by adding surfactants, *Org. Electron.* 14 (6) (2013) 1629–1635.
- [72] M. Yi, et al., Modification of a PEDOT: PSS hole transport layer for printed polymer solar cells, *Sol. Energy Mater. Sol. Cell.* 153 (2016) 117–123.
- [73] W. Zhang, et al., Oleamide as a self-assembled cathode buffer layer for polymer solar cells: the role of the terminal group on the function of the surfactant, *J. Mater. Chem.* 22 (45) (2012) 24067–24074.
- [74] M. Chevrier, et al., Self-assembled conjugated polyelectrolyte-surfactant complexes as efficient cathode interlayer materials for bulk heterojunction organic solar cells, *J. Mater. Chem. A* 3 (47) (2015) 23905–23916.
- [75] Y. Yang, et al., High-performance multiple-donor bulk heterojunction solar cells, *Nat. Photonics* 9 (3) (2015) 190–198.
- [76] S.-W. Heo, et al., Patternable solution process for fabrication of flexible polymer solar cells using PDMS, *Sol. Energy Mater. Sol. Cell.* 95 (12) (2011) 3564–3572.
- [77] K.M. O'Malley, et al., Enhanced open-circuit voltage in high performance polymer/fullerene bulk-heterojunction solar cells by cathode modification with a C60 surfactant, *Adv. Energy Mater.* 2 (1) (2012) 82–86.
- [78] F. Pan, et al., 3D surfactant-dispersed graphenes as cathode interfacial materials for organic solar cells, *Sci. China Mater.* 64 (2) (2021) 277–287.
- [79] F. Znidi, M. Morsy, M.N. Uddin, Recent advances of graphene-based materials in planar perovskite solar cells, *Nanotechnology* 5 (2024) 100061.
- [80] E. Muramoto, et al., Carbon nanotube-silicon heterojunction solar cells with surface-textured Si and solution-processed carbon nanotube films, *RSC Adv.* 6 (96) (2016) 93575–93581.
- [81] F. De Nicola, et al., Record efficiency of air-stable multi-walled carbon nanotube/silicon solar cells, *Carbon* 101 (2016) 226–234.
- [82] L. Yu, et al., Heterojunction solar cells based on silicon and composite films of graphene oxide and carbon nanotubes, *ChemSusChem* 8 (17) (2015) 2940–2947.
- [83] A. Arena, et al., Photovoltaic properties of multi-walled carbon nanotubes deposited on n-doped silicon, *Microelectron. J.* 39 (12) (2008) 1659–1662.
- [84] J. Wei, et al., Double-walled carbon nanotube solar cells, *Nano Lett.* 7 (8) (2007) 2317–2321.